Electronic Supplementary Material (ESI) for Energy & Environmental Science.

Supporting Information For

The low overpotential regime of acidic water oxidation part II: Trends in metal and oxygen stability numbers

Authors: Soren B. Scott[1†], Jakob E. Sørensen[1], Reshma R. Rao[2†], Choongman Moon[1‡], Jakob Kibsgaard[1], Yang Shao-Horn[2], and Ib Chorkendorff[1*]

Contents:

1. Overview of isotope-labeling studies in the OER literature

Table S1. Overview of isotope-labelling experiments to probe lattice oxygen evolution in OER electrocatalysis. Expanded from the compilation in ref. [1] *Table 3.1, where there is further discussion.*

Material	**Sample Preparation**	**Sample Labeling**	**Electrolyte**	**Experiment & Detection**	**Result**	**Citation**
PtO_x	On Teflon DEMS membrane	EC oxidation in 98% $H_2{}^{18}O$	Natural 0.5 M H_2SO_4 or 1.0 M KOH	LSV & DEMS	No excess ^{18}O evolved	Willsau, 1985[2]
Ru and RuO_2	Sputtered on Teflon DEMS membrane	Natural	0.5 M H2SO4 in 90% $H_2{}^{18}O$	CVs & DEMS	Some excess ^{16}O evolved	Wohlfahrt-Mehrens, 1987[3]
Hydrous IrO_x	Thermal decomp. of $HIrCl_6$ on Ti	Natural	1 M HClO4 in 10% $H_2{}^{18}O$	CVs & DEMS	> 1 ML excess ^{16}O evolved	Fierro, 2007 [4](reproduced in Roy, 2018[5])
Nanocrystalline RuO_2 and $Ru_{0.9}Ni_{0.1}O_{2-\delta}$	(co-)dep. on Ti mesh and annealed	Natural	0.1 M HClO4 in 98% $H_2{}^{18}O$	CVs & DEMS	Some excess ^{18}O at high η	Macounova, 2009[6]
Molecular Cobaltate Clusters	Electrodep. CO^{2+} in labeled phosphate buf.	~87% ^{18}O from synth.	Natural phosphate buffer	CP & integral headspace	7-15% of ^{18}O loading evolved	Surendranath, 2010[7]
AuO_x	Au oxidized at 2.0 V in 98% $H_2{}^{18}O$	~98 % ^{18}O from synth.	Natural 1 M $HClO_4$	LSV & OLEMS	~ 1 ML $^{18}O_2$ evolved	DiazMorales, 2013[8]
RuO_2: p.c., (110), (100), (101), (111)	Sputter dep. at 400°C (p.c.) or as received (s.c.)	Oxidized in 98% $H_2{}^{18}O$	Natural 0.1 M KOH or 0.1 M H_2SO_4	CVs & OLEMS	Little to no excess ^{18}O evolved	Stoerzinger, 2017[9]
Spinel Co_3O_4	As-received	Natural	0.5 M KOH in 10% $H_2{}^{18}O$	CVs & DEMS	34% ML excess ^{16}O evolved	Amin, 2017[10]
Spinel Co_3O_4	As-received	Natural	0.5 M KOH in 10% $H_2{}^{18}O$	CVs & DEMS	12% ML excess ^{16}O evolved	Amin, 2017[10]
$LaCoO_3$	Solid-state synthesis	Oxidized in 98% $H_2{}^{18}O$	Natural 0.1 M KOH	CVs & OLEMS	Little to no excess ^{18}O evolved	Grimaud, 2017[11]
$La_{0.5}Sr_{0.5}CoO_{3-\delta}$, $Pr_{0.5}Ba_{0.5}CoO_{3-\delta}$, $SrCoO_{3-\delta}$,	Solid-state synthesis	Oxidized in 98% $H_2{}^{18}O$	Natural 0.1 M KOH	CVs & OLEMS	Some excess ^{18}O evolved	Grimaud, 2017[11]
$Ni_{0.75}Fe_{0.25}O_xH_y$, film	Electrodep.	Natural	0.1 M KOH in 98% $H_2{}^{18}O$	CVs & chip EC-MS	<< 0.1% lattice O evolution	Roy, 2018[5]
7 nm $Ni_{0.75}Fe_{0.25}O_xH_y$, nanoparticles	Cluster source dep: (A) metallic; (B) E.C. ox. in $H_2{}^{18}O$; (C) ox. in ~99% $^{18}O_2$	(A) Natural; (B and C) ~ 50% ^{18}O by LEIS	(A) 0.1 M KOH in 98% $H_2{}^{18}O$; (B and C) Natural 0.1 M KOH	CVs & chip EC-MS, LEIS	<< 0.1% lattice O evolution	Roy, 2018[5]
IrO_2	Sputter dep. with 99% $^{18}O_2$	~ 99% ^{18}O from synth.	Natural 0.1 M $HClO_4$	CP at 25 mA/cm^2 & SFC-OLEMS, SFC-ICP-MS	Little to no excess ^{18}O evolved	Geiger, 2018[12]
$IrO_x{\cdot}yH_2O$ / IrO_2	Sputter dep. $Ir^{18}O_2$, cycled in 97% $H_2{}^{18}O$	~97-99% ^{18}O from synth.	Natural 0.1 M $HClO_4$	CP at 25 mA/cm^2 & SFC-OLEMS, SFC-ICP-MS	Some excess ^{18}O evolved	Geiger, 2018[12]
IrO_2	Sputter dep. with 99% $^{18}O_2$	~ 99% ^{18}O from synth.	Natural 0.1 M $HClO_4$	LSV, CP at 10, 15, and 25 mA/cm^2 & SFC-	Little to no excess ^{18}O evolved	Kasian, 2019[13]

				OLEMS, SFC-ICP-MS		
$IrO_x \cdot yH_2O$ / IrO_2	Sputter dep. Ir, cycled in 97% $H_2{}^{18}O$	~97% ^{18}O from synth.	Natural 0.1 M $HClO_4$	LSV, CP at (10, 15, 25) mA/cm^2 & SFC-OLEMS, SFC-ICP-MS	~50, 90, and 120 (~2, 3, 5) pmol/cm^2/s excess ^{18}O evolved (Ir dissolved)	Kasian, 2019[13]
NiO_xH_y, $NiCoO_xH_y$	Layered double hydride single-sheet growth	Oxidized in 97 % $H_2{}^{18}O$	Natural 0.1 M KOH	CA at 1.65 V_{RHE} & Raman	Most ^{18}O exchanged for ^{16}O	Lee, 2019[14]
$NiFeO_xH_y$, $NiFeCoO_xH_y$	Layered double hydride single-sheet growth	Oxidized in 97 % $H_2{}^{18}O$	Natural 0.1 M KOH	CA at 1.65 V_{RHE} & Raman	Little to no exchange of ^{18}O	Lee, 2019[14]
IrO_2	Sputter dep. with 99% $^{18}O_2$	~ 99% ^{18}O from synth.	Natural 0.1 M $HClO_4$	CP at 1 mA/cm^2 & on-line ICP-MS, ATP	3.5% ML of ^{18}O exchanged for ^{16}O > 0.2-0.3% ML Ir dissolved	Schweinar, 2020[15]
IrO_2	Sputter dep. with 99% $^{18}O_2$	~ 99% ^{18}O from synth.	Natural 1.0 M $HClO_4$	CP at 0.25 mA/cm^2 & chip EC-MS	0.07 (0.3) pmol/cm^2/s excess ^{18}O in O_2 (CO_2)	Scott, 2021[16]
IrO_x / Ir	Sputter dep. Ir metal oxidized in 97 % $H_2{}^{18}O$	~ 97% ^{18}O from synth.	Natural 1.0 M $HClO_4$	CP at 0.25 mA/cm^2 & chip EC-MS	0.3 (3.0) pmol/cm^2/s excess ^{18}O in O_2 (CO_2)	Scott, 2021[16]
$IrO_x \cdot yH_2O$ / IrO_2	Sputter dep. $Ir^{18}O_2$, cycled in 97% $H_2{}^{18}O$	~ 97-99% ^{18}O from synth.	Natural 1.0 M $HClO_4$	CP at 0.25 mA/cm^2 & chip EC-MS	2.3 (16) pmol/cm^2/s excess ^{18}O in O_2 (CO_2)	Scott, 2021[16]
PtO_x / Pt	Pt metal oxidized in 97 % $H_2{}^{18}O$	~ 97% ^{18}O from synth.	Natural 1.0 M $HClO_4$	CP at 0.25 mA/cm^2 & chip EC-MS	0.4 (~0.3) pmol/cm^2/s excess ^{18}O in O_2 (CO_2)	Scott, 2021[16]
RuO_x and IrO_x	Sputter dep. with 99% $^{18}O_2$	~ 90% ^{18}O on surface by LEIS.	Natural 0.1 M $HClO_4$	CP at (0.05, 0.15, 0.5) mA/cm2 & chip EC-MS, LEIS, ICP-MS		This work

2. Elaboration of lattice oxygen definition

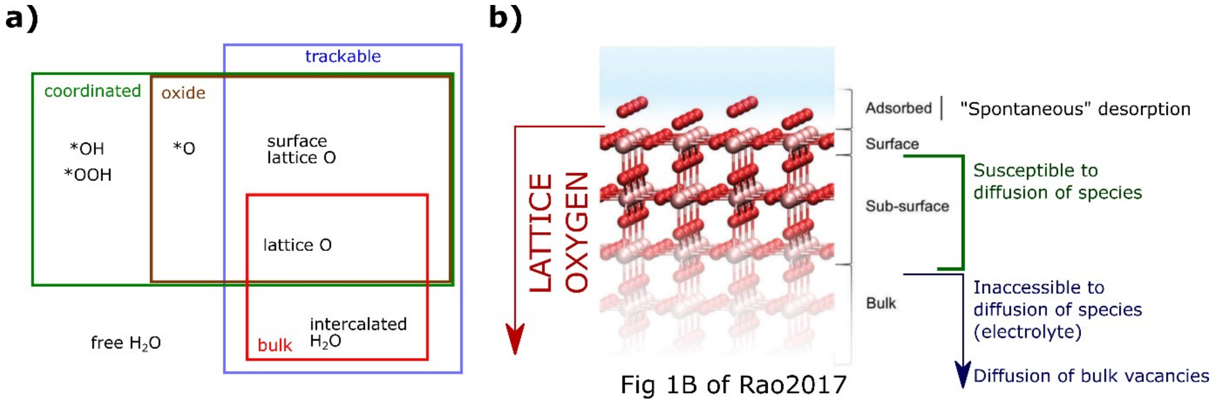

Figure S1. Categorization system of oxygen atoms, described below. The rendering in (b) is from Rao et al, 2017.

- An oxygen atom in a water + metal oxide electrocatalytic OER system can be mapped according to the following characteristics:
    - Coordinated: covalently or ionically bound to a metal atom or covalently bound group of atoms which is bound to a metal atom.
    - Oxide: doubly coordinated, i.e. two formal bonds with metal atoms.
    - Bulk: Inaccessible to the water molecules of the electrolyte
    - Trackable: in the metal oxide which stays in the metal oxide when it is in electrolyte without an applied potential. In other words, oxygen that can retain an isotopic label without reduction of the metal oxide or OER.
- We further propose the following definitions based on these terms (Figure S1)
    - Bulk lattice oxygen: Oxygen atoms which are coordinated, trackable, and bulk
    - Surface lattice oxygen: Oxygen atoms which are coordinated and trackable but not bulk
    - Adsorbed oxygen: Oxygen atoms which are coordinated but not trackable
- Based on the above definitions, and the fact that dissolution of a metal atom can reduce the coordination environment of neighboring oxygen atoms, we reason that:
    - Proof of surface lattice oxygen evolution requires $n_O > n_{diss}$
    - Proof of bulk lattice oxygen evolution requires $n_O > n_{diss}$ *and* $n_O > n_{ML}$
- Thus, isotope labeling studies must be quantitative to be useful. We can map out all prior studies according to these conditions (main-text Figure 1).

3. More annotated EC-MS-ICPMS plots

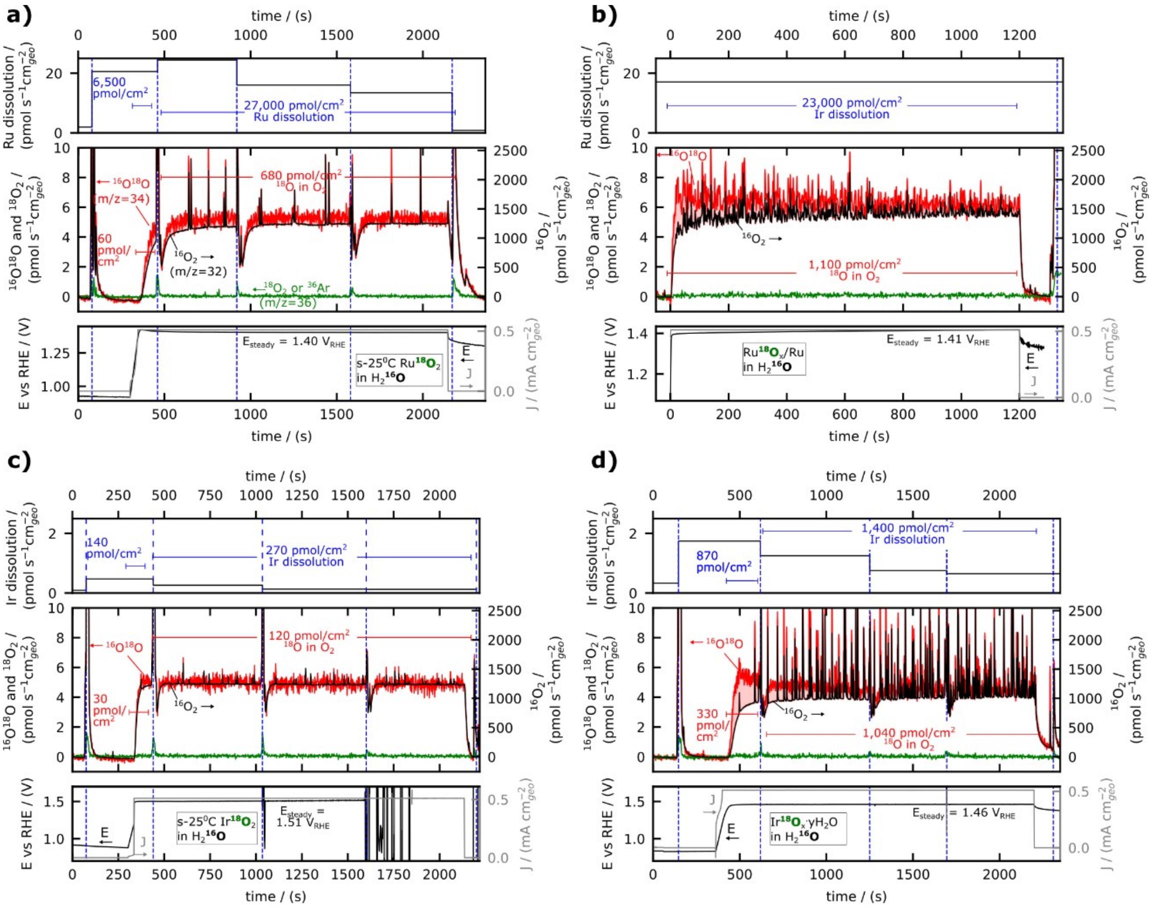

Figure S2. Isotope-tracking plots for OER at 0.5 mA/cm^2 for four samples: ***(a)*** *s-25°C Ru$^{18}O_2$ i.e. RuO_2 sputter-deposited in plasma containing $^{18}O_2$ (the same data as Figure 1b),* ***(b)*** *RuO_x/Ru i.e. a metallic Ru film electrochemically oxidized in labeled electrolyte* ***(c)*** *s-25°C Ir$^{18}O_2$ and* ***(d)*** *Ir$^{18}O_x$.yH_2O, a hydrous amorphous film formed by potential cycling of s-25°C Ir$^{18}O_2$ in labeled electrolyte. The top panel of each plot shows the average metal dissolution rate between sampling times, as measured by ICP-MS. Vertical blue lines indicate electrolyte sampling times (electrolyte was only sampled at the end for Ru$^{18}O_x$/Ru). The middle panel shows in-situ mass spectrometry data on two axes scaled by the natural $^{16}O^{18}O/^{16}O_2$ ratio of 0.4%, such that an isotope signal is seen when the red 16O18O trace (plotted on the left y-axis) lies above the black $^{16}O_2$ trace (right y-axis). The bottom panel shows electrochemical current and potential (reference electrode contact was lost towards the end for RT-Ir$^{18}O_2$, but the applied current was not affected). Integral values for dissolution and lattice oxygen evolution and average values for steady potential are indicated.*

4. Ir dissolution and lattice oxygen reactivity in CO oxidation

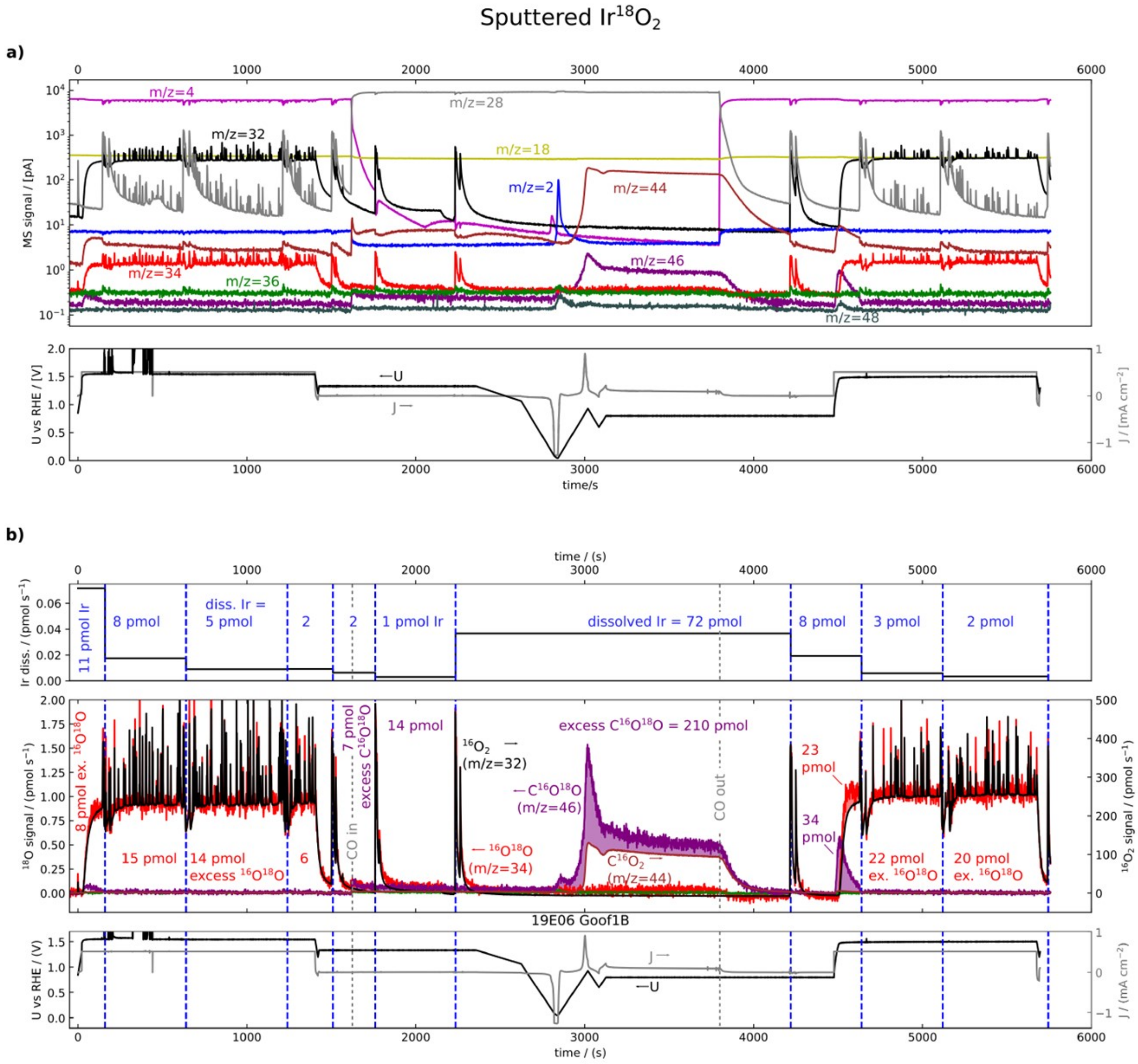

Figure S3. Dissolution (top panels) and lattice oxygen reactivity (middle panels) during a CO oxidation experiment (electrochemical data in bottom panel) on s-25°C IrO_2. The electrolyte is saturated with CO through the chip from ~1600 s until ~3800 s. The ^{18}O-containing isotopes $C^{16}O^{18}O$ (m/z=46) and $^{16}O^{18}O$ (m/z=32) are plotted against the left y-axis while $^{16}O_2$ (m/z=32) and $C^{16}O_2$ (m/z=44) are plotted against the right y-axis. Like Figure 2, the axes are scaled according to the natural isotopic ratio so that any increase of the purple trace ($C^{16}O^{18}O$) above the brown trace ($C^{16}O_2$), like any increase of the red trace ($^{16}O^{18}O$) above the black trace ($^{16}O_2$) is a sign of lattice oxygen incorporation in the respective electrochemical product. See Figure S3 for the raw data.

As a highly interesting side note, we wish to briefly comment on a reaction that we believe shows “True lattice oxygen evolution” as defined in Figure 1, but which is excluded from that figure because the lattice oxygen is evolved in CO_2 rather than in O_2. In reference [16], we showed that lattice oxygen can, under the right conditions, react with carbon monoxide (CO) in electrochemical CO oxidation. Since the reaction reduces the sample, it could also be called an electrochemically assisted reduction of the metal oxide with carbon monoxide. In that work, we showed that several monolayers of ^{18}O from an IrO_2 sample could be evolved in CO_2. However, we did not measure metal dissolution.

Figure S3 shows the results of a CO oxidation experiment with a labeled $Ir^{18}O_2$ sample in unlabeled electrolyte. (The same experiment was not successful for $Ru^{18}O_x$, which showed no oxidation of CO under these conditions.) The mass spectrometry signals for isotopically labeled and unlabeled electrochemical products are plotted on left and right y-axes, respectively, which are scaled according to the natural ratio of $^{18}O^{16}O$ to $^{16}O_2$, which is also the natural ratio of $C^{18}O^{16}O$ to $C^{16}O_2$, such that trackable oxygen in the CO_2 manifests itself as the purple trace ($C^{18}O^{16}O$) rising above the brown trace ($C^{16}O_2$). Starting from the left, the $Ir^{18}O_2$ sample is subject to 20 minutes of OER in He-saturated electrolyte (note that $n_{diss}<n_O<<1$ ML) before CO is introduced at ~2200 s. Then the sample is scanned to 0 V_{RHE} as is necessary to "activate" the surface for CO oxidation and back up to 0.8 V_{RHE} before settling on 0.75 V_{RHE}. The CO_2 signal contains a strong isotopic signal, much stronger than had been observed during OER. Some dissolution is also observed, likely due to the cathodic scan in the same electrolyte sampling interval, as a cathodic scan is known to corrode IrO_2. However, trackable oxygen evolution in CO_2 exceeds metal dissolution by at least a factor 3. Together with our previous work, this establishes that for CO reaction with $Ir^{18}O_2$, we can have $n_O>n_{diss}$ and $n_O>1$ ML.

The reaction of CO reaction with $Ir^{18}O_2$ is also interesting because, together with the OER results, it sheds light on which states of oxygen on the surface of iridium oxides can promote lattice oxygen reactivity. Specifically, trackable oxygen can enter reactive surface states at the potential of CO oxidation, 0.7-0.8 V_{RHE}, even if it is relatively unreactive in surface states at the high potentials needed for oxygen evolution >1.23 V_{RHE}. These potential ranges fit with *OH being oxygen-activating species, because *OH is expected to be on the surface at 0.7-0.8 V_{RHE} but not at OER potentials where the dominant state is expected to be *O (ref. [17]). This is the last piece of the puzzle needed to assemble a combined mechanistic picture of water oxidation, metal dissolution, and trackable oxygen evolution.

5. Additional LEIS results

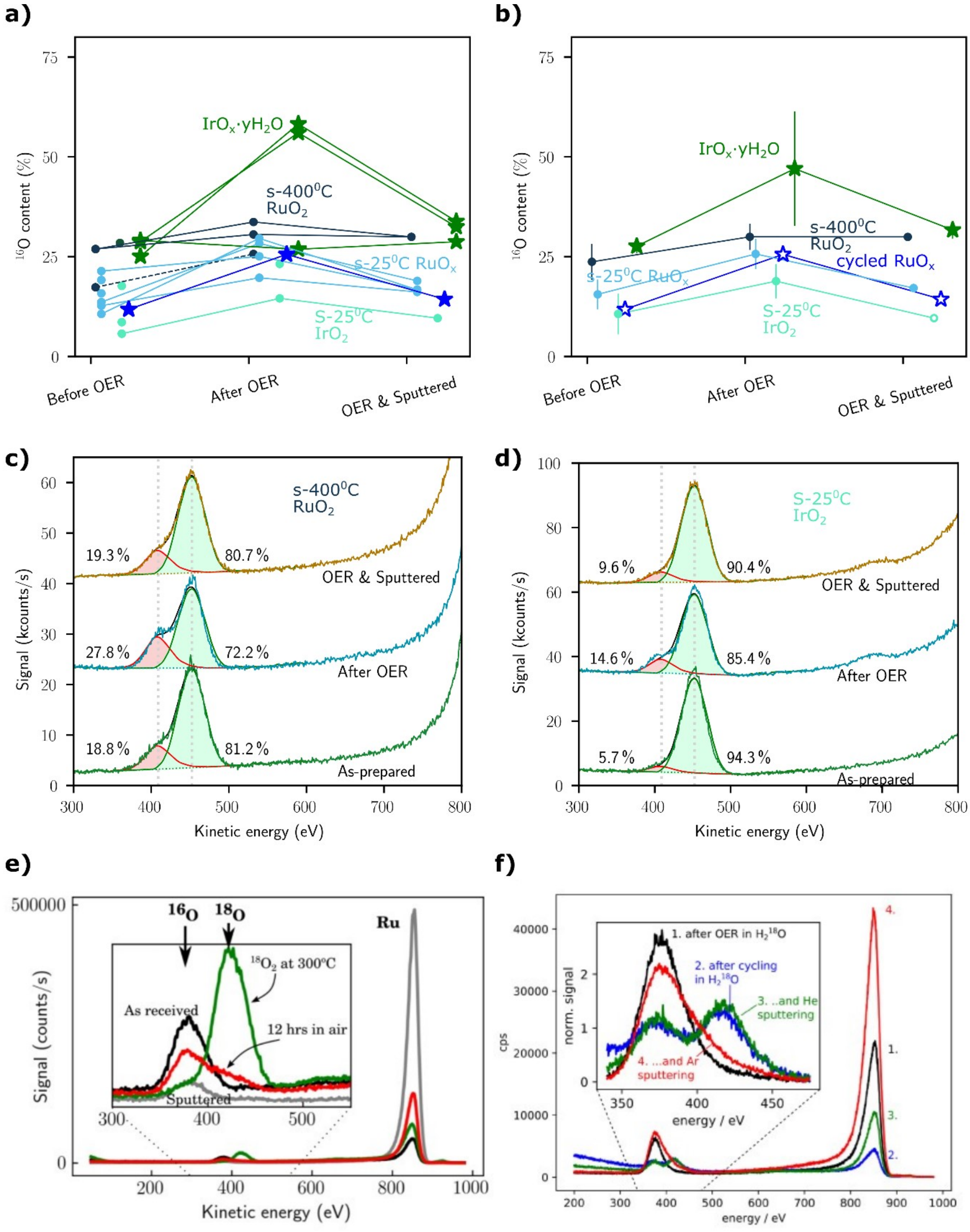

Figure S4 (a-b) LEIS results for all samples. (a) Fitting results for individual spectra (b) Sample types grouped, marker and error bar are mean and standard deviation. (c-d) additional fitted sample spectra. Note that sputter deposition at higher temperature results in higher $^{16}O/^{18}O$ ratios in the as-prepared samples, likely due to contaminant O_2 degassing from the sputter deposition chamber. (e-f) limiting of other labeling procedures. (e) Thermal labeling: oxidizing a Ru film in 18O2 creates an 18-O label (green), but exposure to air adds a 16-O label indicating the oxidation was incomplete. (f) Electrochemical labeling: cycling an RuOx film in 18-O incorporates >50% 18-O into the surface (blue), but the label is likewise "skin-deep", and is removed by sputtering away ~1 ML with argon (red).

6. ICP-MS calibration curves

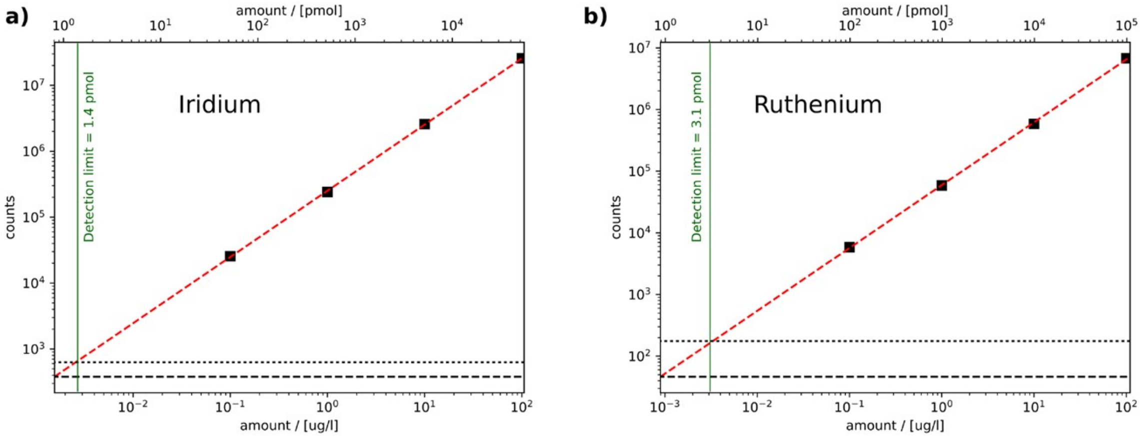

Figure S5 Calibration curves for ICP-MS detection of (a) Ir and (b) Ru. The top x-axes represents the amount of metal originally in a sample from the EC-MS setup, and is scaled to the bottom x-axis according to the equation below. The dashed black line is the mean number of counts in blank measurements, and the dotted black line is that mean plus three times the standard deviation of the number of counts in the blank measurement. The detection limit, defined as where the latter intercepts the calibration curve, is indicated with a green vertical line.

For ICP-MS collection, the electrolyte in the cell is sucked out with a syringe while new electrolyte flows in from an electrolyte delivery tower. The old electrolyte stored in an Eppendorf tube and the syringe is re-inserted. This results in electrolyte samples of ~0.5 ml in Eppendorf tubes. For study with ICP-MS, the raw samples are first diluted to a standard volume of 1 ml with 2% HNO_3, 0.1 ml of this is then diluted to 10 ml with 2% HNO_3, which is the ICP-MS sample. The concentration of this ICP-MS sample is then as if all of the metal dissolved during the experiment were diluted in 100 ml. The amount of metal n^i (typically stated in pmol) can then be determined from its mass concentration c_m^i in the ICP-MS sample (typically stated in µg per l which is numerically equivalent to ppb) by

$$n^i = 100\,[\mathrm{ml}]\frac{c_m^i}{M^i}\,,$$

where M^i is the molar mass of element i.

To determine c_m^i from the raw signal (in counts) requires calibration. A dilution series (typically 0.1, 1, 10, and 100 µg/l) is prepared from a standard stock solution. These are measured together with the samples and intervening measurements a blank solution (2% HNO_3 in water with no metals). The calibration curve is made by drawing a line of best fit through the counts vs concentrations of this dilution series on a log-log plot (the slope of this line should be 1).

7. Additional isotope tracking plots (database contents)

See https://github.com/ixdat/LowOverpotentialRegime

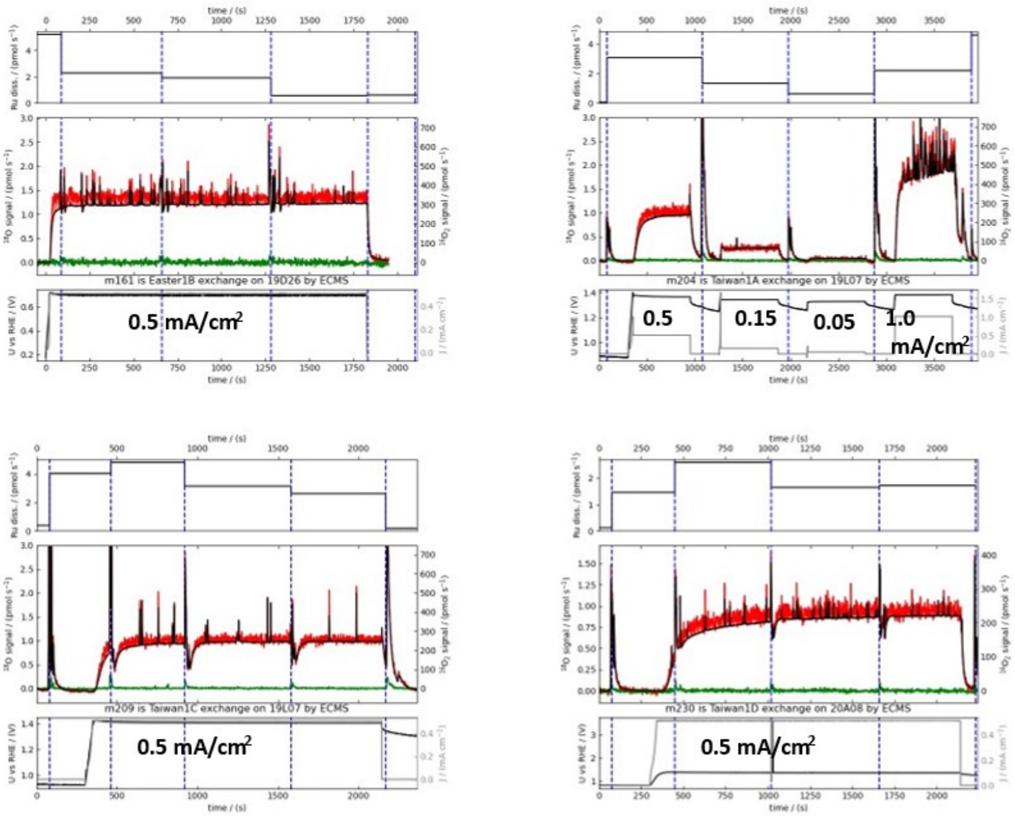

Figure S6. Ru$^{18}O_2$ sputter deposited at RT

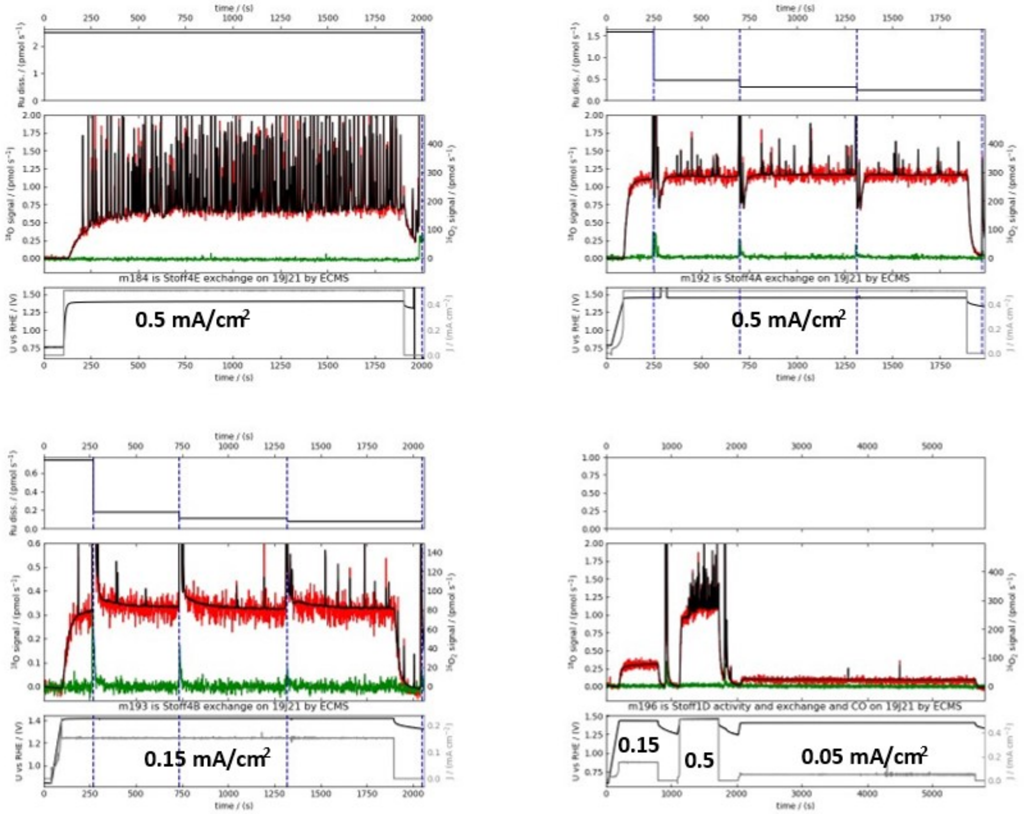

Figure S7. Ru^{18}O$_2$ sputter deposited at 400 C

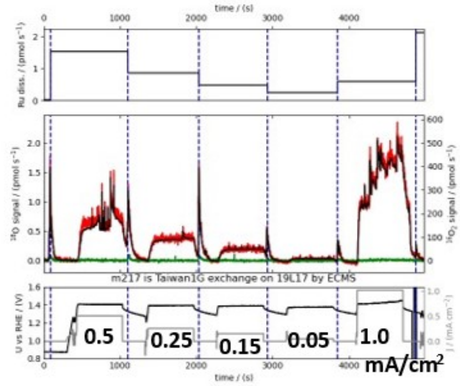

Figure S8. Ru^{18}O$_2$ cycled in H$_2$^{18}O

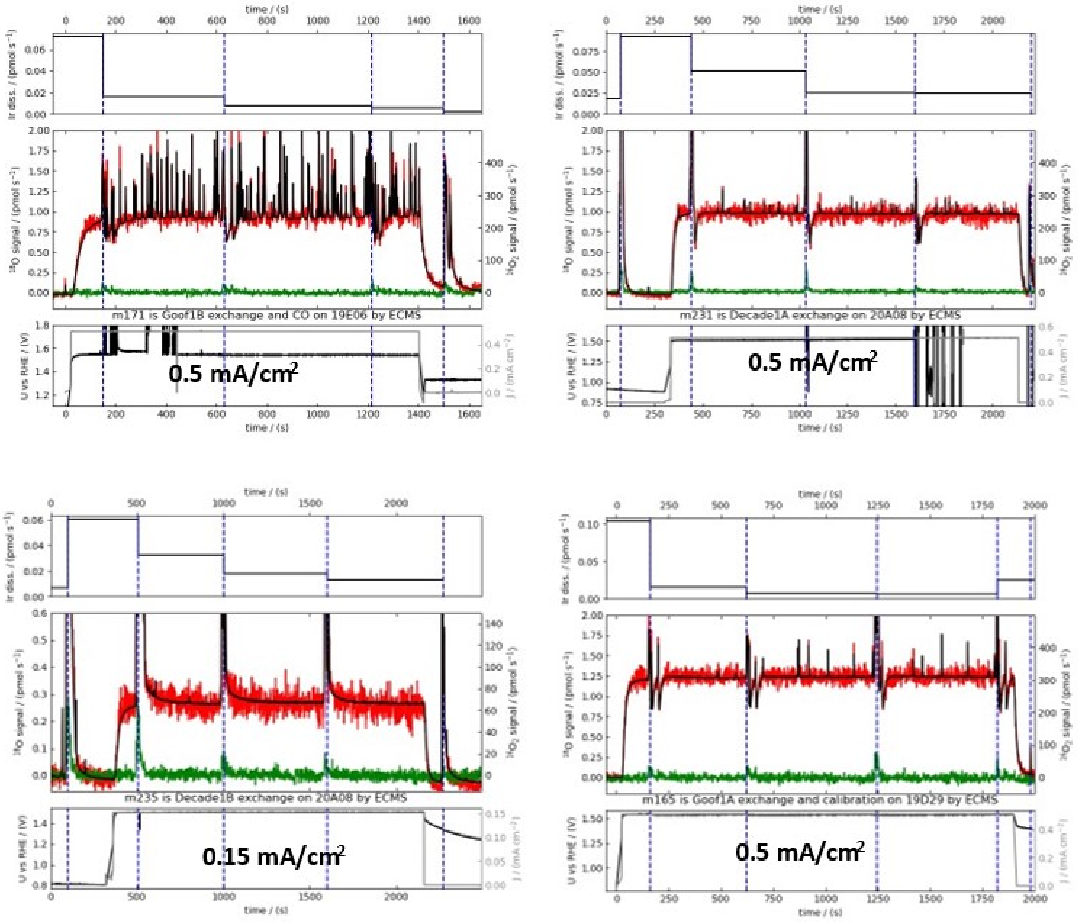

Figure S9. Ir^{18}O$_2$ sputter deposited at RT

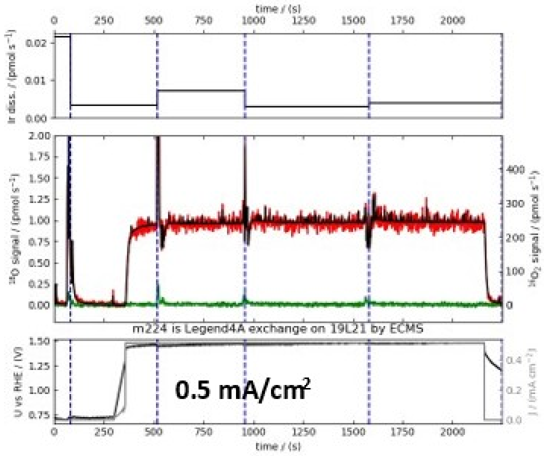

Figure S10. Ir^{18}O$_2$ sputter deposited at 400 C

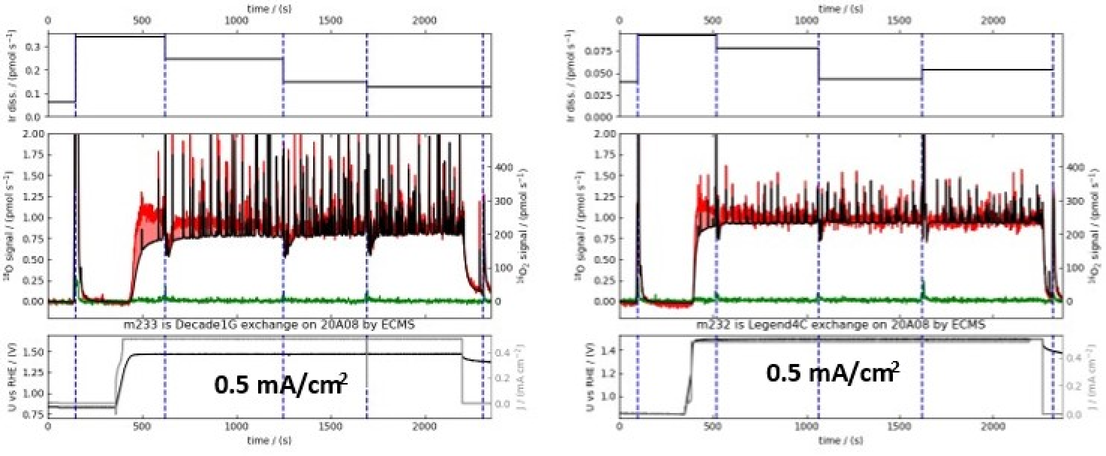

Sputtered at RT

Sputtered at 400 C

Figure S11. Ir^{18}O$_2$ cycled in H$_2{}^{18}$O

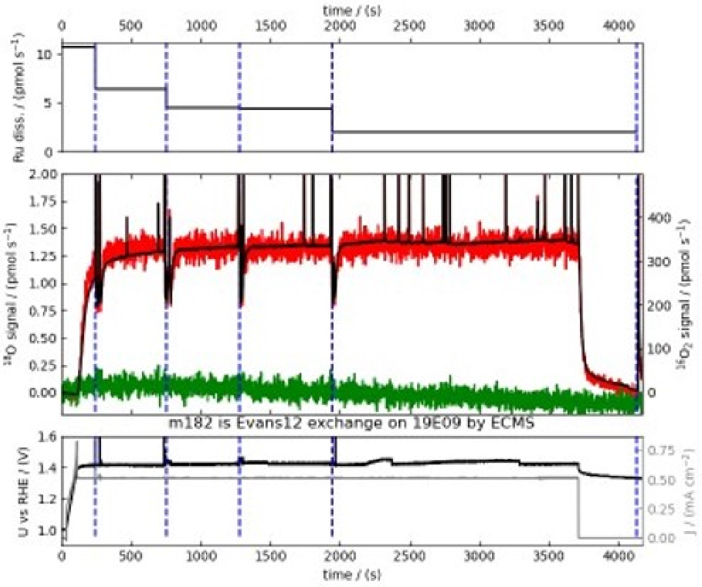

Figure S12. Electrochemically labelled Ru foam

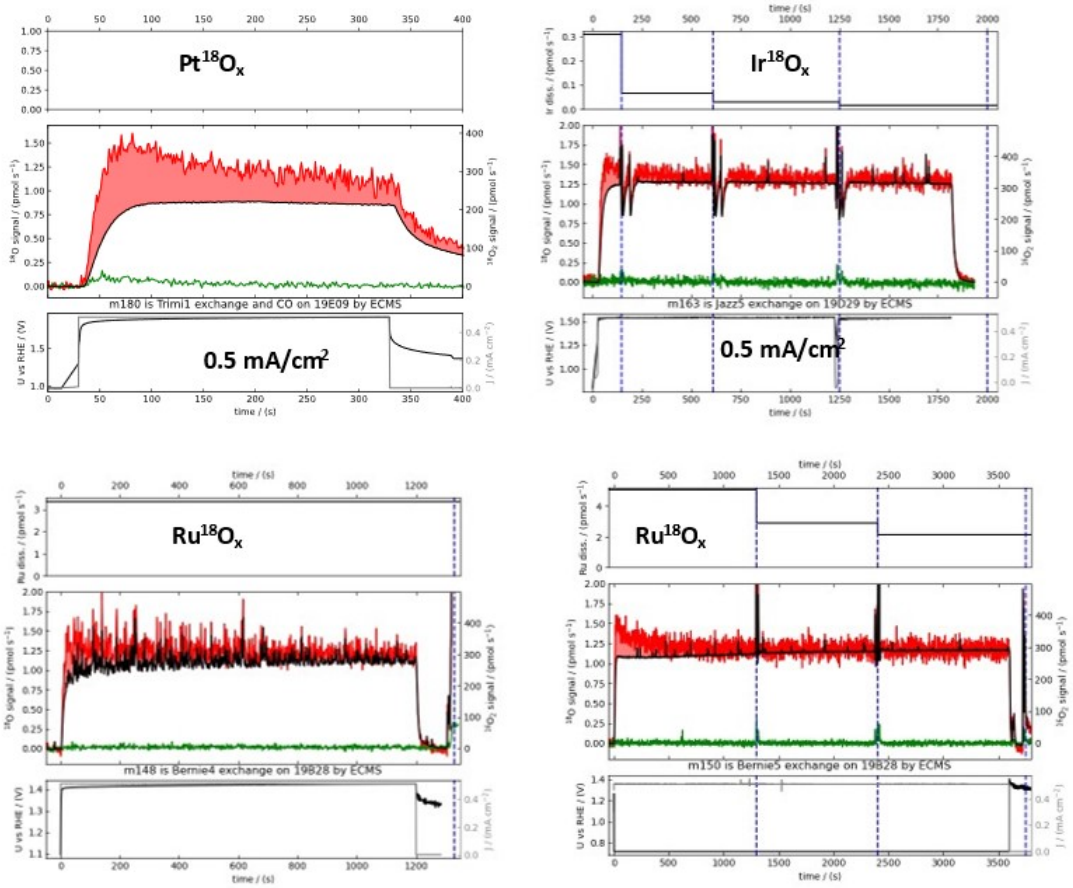

Figure S13 Electrochemically grown 18O oxide layers

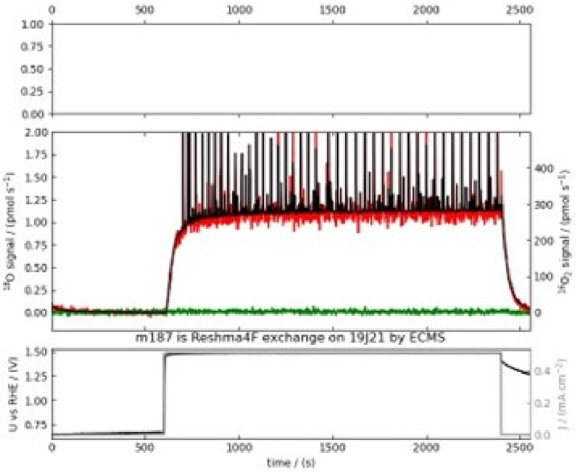

Figure S14. Ru^{16}O$_2$ control (one of many controls)